Truncation Effect of a Three-Dimensional Compound Parabolic Concentrator on the Solar Flux at the Input of the Receiver of a 30 kWe Solar Tower Power Plant

Kory Faye[1(✉)], Mactar Faye[1,2], El Hadji Ibrahima Cissé[2], Ababacar Thiam[1,2], and Vincent Sambou[2]

[1] Research Group Energetic System and Efficiency, Department of Physic, Alioune Diop University of Bambey, B.P. 30, Bambey, Senegal
kory.faye@uadb.edu.sn

[2] Laboratory of Water, Energy Environment and Industrial Processes, Polytechnic School, Cheikh Anta Diop University, S-10700 Dakar-Fan, Senegal

Abstract. The length of compound parabolic concentrator affects the performance of solar tower power plant. This study investigates the truncation effect of a three-dimensional compound parabolic concentrator (3D-CPC) on the solar flux at the input of the solar receiver of a 30 kWe solar tower power plant. Firstly, the three-dimensional compound parabolic concentrator (3D-CPC) is firstly sized and designed in SolidWorks software. Then, the 3D-CPC is meshed in Ansys Meshing into 2516 elements before being designed in Soltrace software. Finally, Monte Carlo ray racing (MCRT) method is used to simulate the operation of the solar tower power plant with the 3D-CPC truncated at 0°, 35°, 40° and 55°. The optical simulation results showed that the 3D-CPC increases the concentration ratio by a factor of 4.91 with an optical efficiency of 80.12%. The 3D-CPC truncated at 35° collected a higher solar flux than the others 3D-CPC. This shows that the truncation of 3D-CPC has effect on the solar flux at the input of the receiver.

Keywords: Truncation effect · Tree-dimensional compound parabolic concentrator · Solar flux · Solar receiver

1 Introduction

Solar energy source is considered one of the most renewable energy sources because of its cleanliness, abundance and positive impact on the environment [1]. It can be used for electricity production by two technologies such as Photovoltaic solar panels and Concentrated Solar Power (CSP) [2]. The CSP is the most promising technology due to its high efficiency and its advantage in storing thermal energy [3, 4]. Among the CSP technologies, Solar Tower Power Plant (STPP) is more advantageous for electricity production

A. D. Mambo et al. (Eds.): InterSol 2022, LNICST 449, pp. 237–250, 2022.
https://doi.org/10.1007/978-3-031-23116-2_20

because of its high efficiency and low capital cost [2]. However, the density of solar energy is generally affected by factors related to its intermittent nature such as weather conditions, seasons [5, 6]. This is why, concentrating solar systems are usually equipped with uniaxial or biaxial solar tracking devices to improve their performance. However, solar tracking devices require high control accuracy and considerable investment [5, 7].

Non-imaging concentrator such as three-dimensional compound parabolic concentrator (3D-CPC) can be used in solar tower power plants to eliminate solar tracking systems and thus reduce investment costs [8, 9]. In addition, the use of 3D-CPC can increase the concentration of the solar rays at the input of the receiver [10]. Thus, 3D-CPCs are attracting increasingly attention from researchers because of its importance in collecting solar flux with high efficiency in STPPs [11]. However, the major disadvantage of a 3D-CPC is that it is very long compared to its inlet aperture diameter. This disadvantage should be taken into account when designing a 3D-CPC using STPPs to achieve efficiency, economy, and lightness [12].

Many researchers have studied the 3D-CPC used in STPP. Some of them have focused on truncation to improve the geometric dimensions of 3D-CPC. Winston R. [13] show a relationship between the truncation ratio and the length/aperture ratio with different half acceptance angles. Ari Rabl [14] studied the truncation of a 3D-CPC based on the average number of reflections. He showed that the truncation ratio could be selected based on the average number of reflections and the geometric concentration ratio.

Others researchers have studied the performance of 3D-CPCs by in STPPs. G. Dai et al. [15] studied the solar concentrating performance of a dish concentrator (DC) using a truncated 3D-CPC by the MCRT method. For a DC with a tilt angle of 45°, the numerical results show that the interception efficiency (η_{int}) is about 4.0% higher than that of the CPC-DC, but the concentration ratio of the CPC-DC is twice that of the DC. Lipinski and Steinfeld [16] proposed an annular 3D-CPC to capture and concentrate the spilled solar radiation, the transmission efficiency (τ) varying with the angle (θ) of incidence was numerically simulated using the MCRT method. Recently, L. Li et al. [10] designed a 3D-CPC for high-temperature solar thermochemical applications, irradiated by a high-flux multisource solar simulator. Optical simulations showed that 3D-CPC increases the concentration ratio by a factor of 4.1 at 85.4% optical efficiency (η_{opt}), reduces the spilling losses (η_{spil}) from 78.9% to 32.1%, and reduces the no-uniformity of the solar flux on the target surface. L. Li et al. [17] studied the thermal and economic performances of a solar central receiver system equipped with 3D-CPC. Using an MCRT model, a heat transfer model, and a cost model based on System Advisor Model (SAM), they showed that a 3D-CPC can improve the thermal (η_{th}) and economic (LCOX) performances of the system only at temperatures between 900 K and 1200 K. However, the truncation effects of these 3D-CPCs have not been studied.

The above-mentioned research work has investigated the truncation effects of 3D-CPCs on the geometrical dimensions and studied the thermal and economic performances of the 3D-CPCs by using central receiver. As far as l know, no study has yet been performed on the truncation effects of a 3D-CPC on the solar flux at the input of the receiver. The objective of this study is to investigate the truncation effect of a 3D-CPC on the solar flux at the input of the receiver of a 30 kWe solar tower power plant.

To achieve this objective, a two-dimensional CPC (2D-CPC) is sized firstly and designed in a three-dimensional paraboloid form in SolidWorks software. Then, the 3D-CPC is meshed using Ansys Meshing to calculate the different parameters needed for its design in Soltrace software [18]. Finally, the optical simulations of the STPP with a 3D-CPC truncated at 0°, 35°, 40° and 55° are achieved by the MCRT method. The average solar flux at the input of the receiver is collected for each 3D-CPC truncated during different periods of the year to visualize the truncation effect.

2 Materials and Methods

2.1 3D-CPC description

The 3D-CPC described in Fig. 1 is a no-imaging solar concentrator formed by rotating the cross-section of a 2D-CPC around the optical axis (z) [14]. The half acceptance angle (θ_a) is the angle formed by the optical axis and the line (AC). The half acceptance angle is defined as the maximum angle of incidence that allows incident rays at the inlet aperture of the 3D-CPC to be reflected to the receiver [8]. However, the rays with incidence angles larger than half acceptance angle fail to reach the receiver.

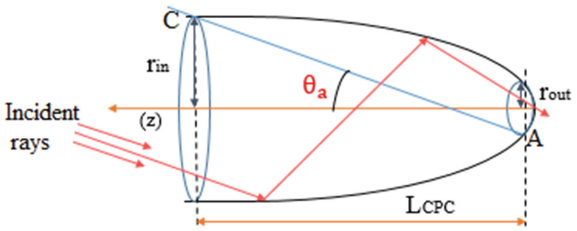

Fig. 1. Schematic diagram of a 3D-CP below the illustration.

2.2 3D-CPC Sizing

The two parameters determining the geometry of a 3D-CPC are the half acceptance angle (θ_a) and the inlet aperture radius (r_{in}). The outlet aperture radius (r_{out}) of the 3D-CPC can be determined by [19, 20]:

$$r_{out} = r_{in}\sin(\theta_a) \tag{1}$$

The length (L_{CPC}) of the 3D-CPC is calculated by the following relationship:

$$L_{CPC} = \frac{f\cos(\theta_a)}{\sin^2(\theta_a)} \tag{2}$$

where f is the focal distance of the 3D-CPC given by the following expression:

$$f = r_{out}(1 + \sin(\theta_a)) \tag{3}$$

In a full 3D-CPC, the upper part is almost parallel to the optical axis (described in red in Fig. 2), thus contributing very low in concentrating solar rays to the receiver. Therefore, the full 3D-CPC can be truncated to a certain length [21]. The 3D-CPC truncated is now defined by three parameters which are the half acceptance angle, the outlet aperture radius and the vertex angle (ϕ_T) which is called the truncation angle (see Fig. 2).

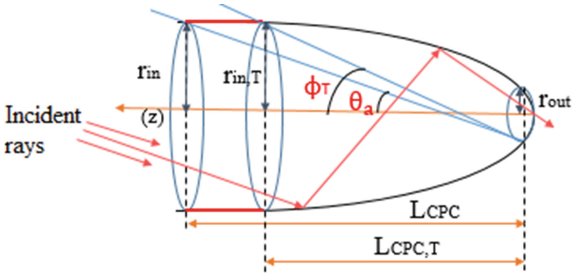

Fig. 2. Schematic diagram of a 3D-CPC showing the upper part parallel to the optical axis

The inlet aperture radius ($r_{in,T}$) and the length ($L_{CPC,T}$) of the 3D-CPC truncated are given by Equations. 4 and 5 respectively [22]:

$$r_{in,T} = \frac{f\sin(\phi_T - \theta_a)}{\sin^2(\phi_T/2)} - r_{out} \tag{4}$$

$$L_{CPC,T} = \frac{f\cos(\phi_T - \theta_a)}{\sin^2(\phi_T/2)} \tag{5}$$

The truncation ratio (r_T) of the 3D-CPC is defined as the ratio of the truncated length to the real length. It is given by:

$$r_T = \frac{L_{CPC,T}}{L_{CPC}} \tag{6}$$

2.3 3D-CPC Design

The method developed by Craig K. et al. in [23] to design a complex solar receiver in Soltrace, is used in this study to design the 3D-CPC. The sizes of the 2D-CPC are used to design the 3D-CPC in SolidWorks software. The 3D-CPC is then meshed using Ansys Meshing with a triangular mesh as described in Fig. 3 [24]. Afterwards, two files containing mesh information are generated by the Ansys Meshing. One contains the elements (triangles) and their nodes (N_1), (N_2), and (N_3) and the other contains the nodes and their coordinates (x, y, z) (see Fig. 3).

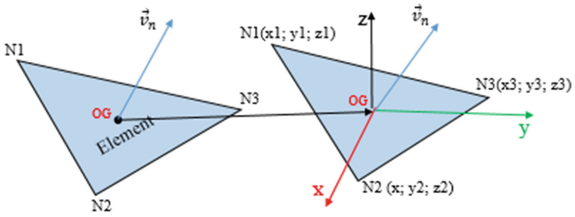

Fig. 3. Mesh element with the nodes of each corner and their coordinates

Thus, the means parameters to define a triangular element in Soltrace are the coordinates of the centroids (OG) and the aim points of each element. The centroid of an element is chosen as the reference point. This reference point is obtained by averaging the coordinates of the three nodes of each element. The coordinates of the reference point are used as input values for the x, y and z coordinates in the stage section of Soltrace. The element is then translated back to the origin by subtracting the reference point coordinates of each node. The relationship that calculates the coordinates of the element after the translation is given by [24]:

$$\begin{pmatrix} x \\ y \\ z \end{pmatrix}_{NiG} = \begin{pmatrix} x \\ y \\ z \end{pmatrix}_{G} - \begin{pmatrix} x \\ y \\ z \end{pmatrix}_{Ni} \tag{7}$$

The normal vector ($\vec{v}_n$) of the element can be calculated by the cross product of the vectors of two nodes. Equation 8 is used to calculate the normal vector of an element.

$$\vec{V}_n = (y_1z_2 - z_1y_2)\vec{i} + (z_1x_2 - x_1z_2)\vec{j} + (x_1y_2 - y_1x_2)\vec{k} \tag{8}$$

The norm of the normal vector ($\|\vec{v_n}\|$) can be calculated by the following expression:

$$\|\vec{v_n}\| = \begin{Bmatrix} \left(\frac{v_{nx}}{\sqrt{v_{nx}^2+v_{ny}^2+v_{nz}^2}}\right) \\ \left(\frac{v_{ny}}{\sqrt{v_{nx}^2+v_{ny}^2+v_{nz}^2}}\right) \\ \left(\frac{v_{nz}}{\sqrt{v_{nx}^2+v_{ny}^2+v_{nz}^2}}\right) \end{Bmatrix} \tag{9}$$

The coordinates of the aim point of each element can be calculated by the sum of the coordinates of the reference point and the normal vector:

$$\begin{pmatrix} x \\ y \\ z \end{pmatrix}_{Ap} = \begin{pmatrix} x \\ y \\ z \end{pmatrix}_{G} + \begin{pmatrix} x \\ y \\ z \end{pmatrix}_{Vn} \tag{10}$$

3 Results and Discussion

3.1 Results of sizing

The basic geometrical parameters of the 3D-CPC, including the half acceptance (θ_a) angle of 12.5° and the inlet aperture radius (r_{in}) of 0.70 m, are determined by means of optical simulations. From these values, the size results of the 3D-CPC are given in Table 1.

Table 1. Sizes of the three-dimensional compound parabolic concentrator

Parameters	Values (m)
Outlet aperture radius (r_{out})	0.15
Focal distance (f)	0.18
Length (L_{CPC})	3.84

3.2 Results of design

A code is developed in Matlab software to calculate the size of the 3D-CPC and to plot its parabolic profile as shown in Fig. 4. The 2D-CPC consists of two parabolic reflectors symmetrical to the optical axis (z). Thus, the shape of the 3D-CPC is obtained by the rotation of the 2D-CPC cross section around the optical axis of the 2D-CPC. Figure 5 shows the shape of the 3D-CPC designed by SolidWorks software.

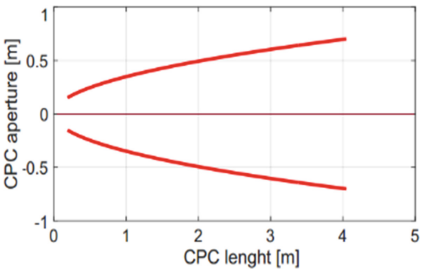

Fig. 4. 2D-CPC parabola profile

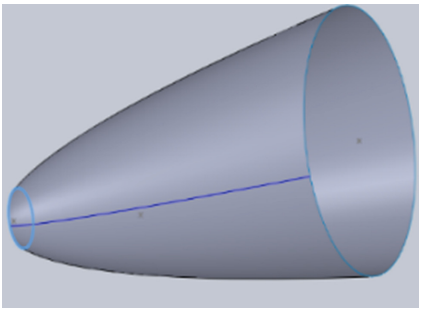

Fig. 5. 3D-CPC design in SolidWorks

The shape of the 3D-CPC is complex and its design in Soltrace is very problematic. Indeed, Soltrace offers only the users the possibility to design standard geometrical shapes such as circles, triangles, and flat rectangles or curved shapes such as cylinders, cones… [25]. For this reason, the 3D-CPC is meshed in Ansys Meshing by a fine triangular mesh. Figure 6 shows the 3D-CPC meshed into 2516 elements (i.e., small triangles in Fig. 6). Then, the mechanical APDL tool of Ansys Workbench is used to

edit the two mesh files. One of the files contains the elements and the nodes of the different corners of the element (N_1, N_2, and N_3) and the other file contains the nodes and their coordinates (x, y, and z) in disorder. Therefore, a script is developed under RStudio software to associate and tidy the elements and nodes with their respective coordinates. After, the coordinates of the centroids (x_G, y_G, z_G) and the aim points ($x_{Aimpoint}, y_{Aimpont}, z_{Aimpoint}$) of each element are calculed. These coordinates are used to design the 3D-CPC in Soltrace (see Fig. 7).

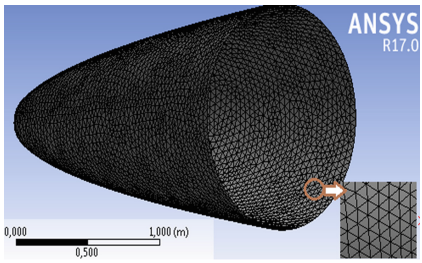

Fig. 6. 3D-CPC mesh in Ansys Meshing

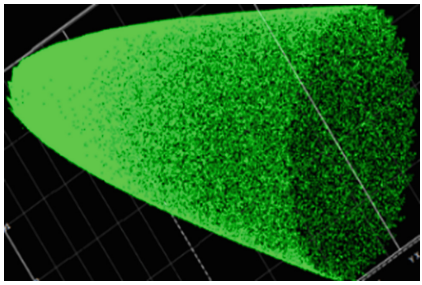

Fig. 7. 3D-CPC design in Soltrace

The dimensions of the different subsystems of 30 kWe solar tower power plant are all interdependent parameters that also make the design and positioning of the 3D-CPC complex in Soltrace software. The sizes of the different parameters of the solar field of the 30 kWe STPP found in our previous work [26], are used in this study. The characteristics of the different subsystems of STPP are shown in Table 2.

Table 2. Characteristics of the STPP subsystems 3D-CPC Orientation South.

Subsystems	Parameters	Values
Heliostat	Form	square
	Number	175
	Area (Single-facet)	2 m^2
	Height	1.5 m
3D-CPC	Orientation	South
	Height	26 m
	Inlet aperture radius	0.7 m
	Outlet aperture radius	0.15 m
	Focal distance	0.18 m
	Length	3.84 m
	Tilt angle	55°
Receiver	Form	Circular
	Aperture radius	0.15 m

Figures 8 and 9 show the design of the solar tower power plant without 3D-CPC and with 3D-CPC, respectively, in Soltrace. The parameters listed in Table 2 are taken into account in the optical simulations. For the heliostats and the 3D-CPC, a reflectivity (ρ) of 0.95, a transmitivity (τ) of 0, a slope error (σ_{slop}) of 1 mrad and a specularity error (σ_{spec}) of 0.9 are also taken into account in the optical simulations. In addition, an absorptivity (α) of 0.95, a slope error of 0.90 mrad, and a specularity error of 0.90 are assigned to the solar receiver. For the sun shape, a Pillbox distribution (θ_{sun}=4.65 mrad) is selected. 100,000 solar rays are launched for the optical simulation to determine the average solar flux at the inlet and exit of the 3D-CPC. Figure 10 shows the multiple reflections of solar rays inside the 3D-CPC.

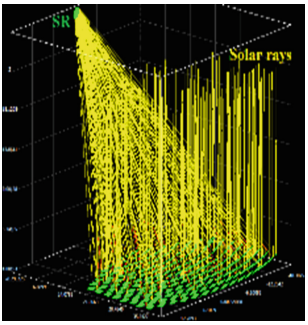

Fig. 8. STPP without 3D-CPC

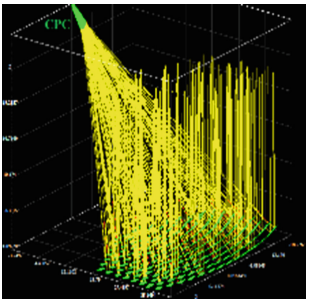

Fig. 9. STPP with 3D-CPC

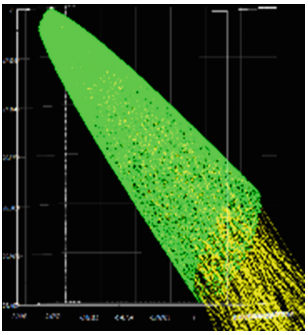

Fig. 10. Solar rays in the 3D-CPC

Figure 11 shows the average solar flux collected at the receiver as a function of time for the STPP with 3D-CPC and without 3D-CPC. The average solar fluxes at 12 h: 00 are 98.79 kW/m^2 without 3D-CPC and 496.89 kW/m^2 with 3D-CPC, i.e., a difference of about 80.12%. This difference is due to the non-uniformity of the solar flux distribution on the receiver without 3D-CPC. This non-uniformity solar flux distribution leads to hot spots on the surface of the receiver and reduces the amount of solar flux. To increase the solar flux and reduce the hot spots, a 3D-CPC is used. Figure 12 shows the average solar flux collected at the input and output of the 3D-CPC as a function of time. The average solar flux collected at the input of the 3D-CPC is 100.99 kW/m^2. Thus, the optical simulations show that the 3D-CPC increases the concentration ratio by a factor of 4.91.

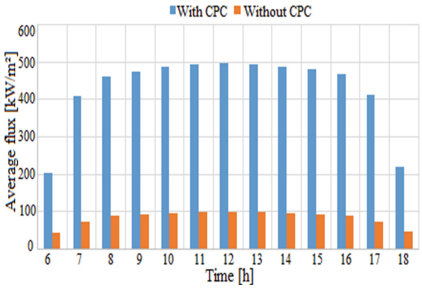

Fig. 11. Average solar flux collected as a function of time (summer solstice)

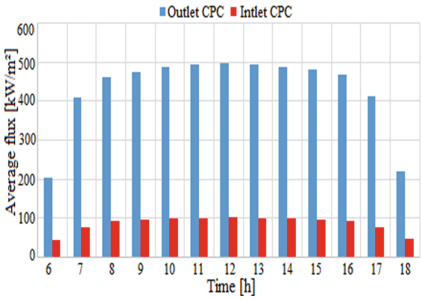

Fig. 12. Average solar flux as a function of time (summer solstice)

3.3 Results of Truncation Effect

The length of the full 3D-CPC is 3.84 m, which is much longer than its inlet aperture diameter of 1.4 m. For this reason, the 3D-CPC is truncated at 0° (untruncated), 35°, 40° and 55°. The truncation ratio (r_T) of the 3D-CPC is shown in Fig. 13. It can be seen that the truncation ratio decreases when the truncation angle increases. This means that as the truncation angle increases, the length of the 3D-CPC truncated decreases. Figure 14 shows the 3D-CPC truncated at 0°, 35°, 40° and 55°. In this figure, it is clear that if the truncation angle increases from 35° to 55°, the length decreases from 2.62 m to 1.40 m. The truncation also widens the inlet aperture and increases its capacity to collect solar rays that were outside of the nominal half acceptance angle.

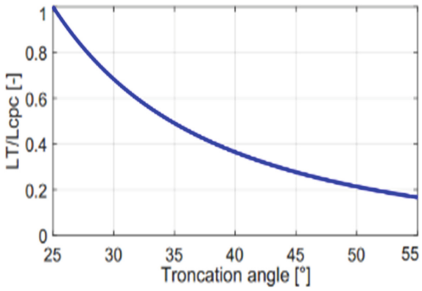

Fig. 13. Truncation ratio via truncation angle of 3D-CPC

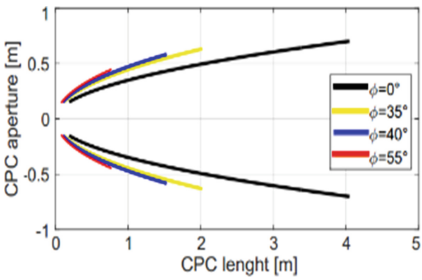

Fig. 14. Parabolic profiles of 2D-CPC at 0°, 35°, 40° and 55°

Figure 15 shows the 3D-CPC truncated at 0°, 35°, 40° and 55°. It can be seen that the truncation decreases the length and increases the inlet aperture of the 3D-CPC. The truncation changes the field of view of the 3D-CPC and allows some solar rays, beyond the nominal half acceptance angle, to reach the receiver. The average solar flux is collected for each 3D-CPC at 12 h: 00 during the summer solstice. Table 3 gives the average solar flux at the input of the receiver and the size of each 3D-CPC. The 3D-CPC truncated at 35° provides a higher average solar flux than the other 3D-CPCs.

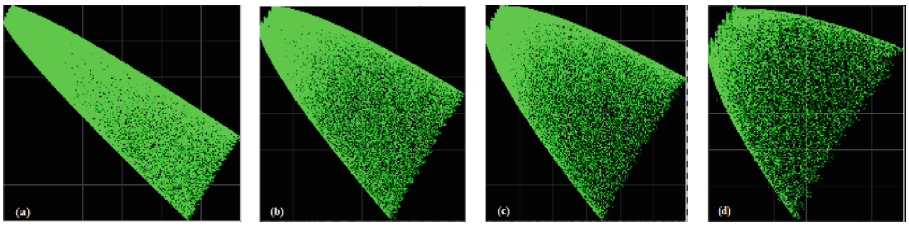

Fig. 15. Three-dimensional compound parabolic concentrator truncated at 0° (a), 35° (b), 40° (c), and 55° (d)

Table 3. Performances of each 3D-CPC

Truncation angle (°)	Length (m)	Inlet aperture radius (m)	Average solar flux (kW/m^2)
0	3.84	0.70	495.82
35	2.62	0.68	514.02
40	1.88	0.63	479.00
55	1.40	0.58	466.76

The results shown in Table 3 are not sufficient to properly assess the effects of the truncation of a 3D-CPC on the solar flux. For this reason, the optical simulations were performed during four periods of the year (spring equinox, autumn equinox, winter solstice, and summer solstice). Figure 16 shows the average solar flux collected at the input of the receiver as a function of time for each 3D-CPC during the four periods. The optical simulation results show that the 3D-CPC truncated at 35° collects a higher average solar flux than the other 3D-CPC for each period. The solar rays that enter the 3D-CPC with incidence angles smaller than the acceptance angle, reach the receiver either directly or after several reflections from the 3D-CPC walls. On the one hand, when the length of the 3D-CPC is long (i.e., the untruncated 3D-CPC), the reflections of the solar rays inside the 3D-CPC are more numerous and therefore the intensity of some solar rays decreases. On the other hand, when the length of 3D-CPC is small (i.e., for 3D-CPCs truncated at 40° and 55°), spilling losses appear. In addition, most of the incident solar rays on the input of the receiver are rejected to the outside after reflection. This shows that the truncation of a 3D-CPC has effects on the solar flux at the input of the receiver.

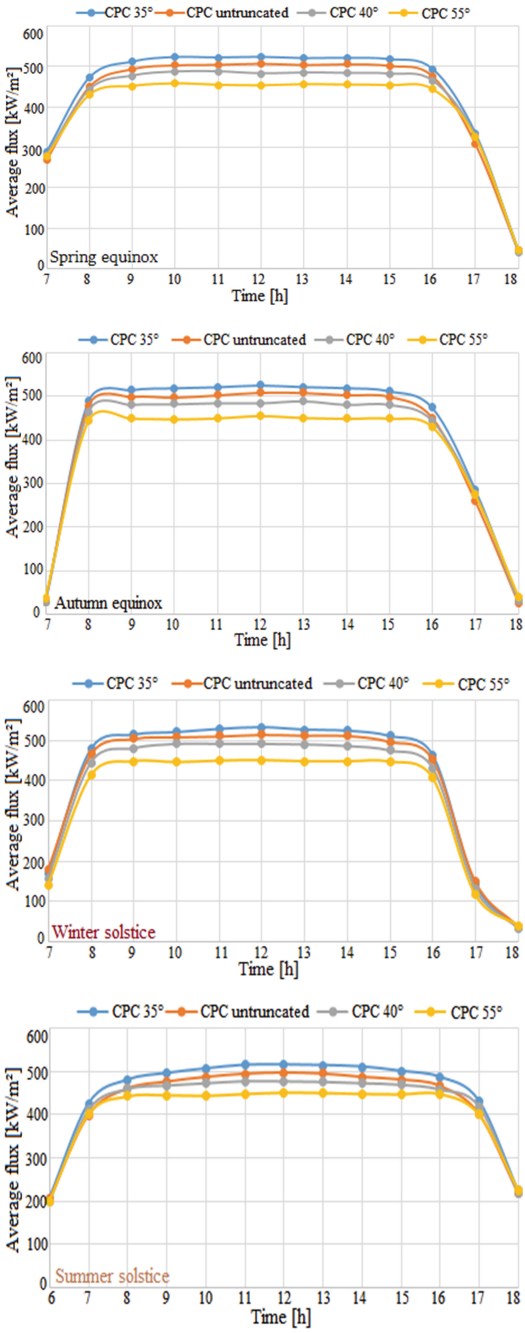

Fig. 16. Average solar flux collected at the input of the receiver via time for each 3D-CPC during four periods

4 Conclusion

A three-dimensional compound parabolic concentrator is a very interesting solar collector technology for various applications because it does not require a solar tracking system. The objective of this study was to investigate the truncation effect of a 3D-CPC on the solar flux at the input of the receiver of a 30 kWe solar tower power plant. To achieve this objective, the three-dimensional compound parabolic concentrator (3D-CPC) is firstly sized and designed in SolidWorks software. Then, the 3D-CPC is meshed into 2516 elements in Ansys Meshing to calculate the different parameters needed for in its design in Soltrace. Finally, the Monte Carlo ray-tracing (MCRT) method is used to simulate the operation of 30 kWe STPP with the 3D-CPC truncated at 0°, 35°, 40° and 55°. The optical simulation results showed that the 3D-CPC increases the solar concentration ratio by a factor of 4.91 with an optical efficiency of 80.12%. The 3D-CPC truncated at 35° collected a higher solar flux than the others 3D-CPC. This shows clearly that the truncation of a 3D-CPC has effects on the solar flux at the input of the receiver.

Thus, the 3D-CPC truncated at 35° whose length, inlet, and outlet radius are 2.62 m, 0.68 m, and 0.15 m, respectively, will be used to study the heat transfer inside the volumetric solar receiver in our future study.

Nomenclature.

θ_a : Acceptance angle (°)
θ: Incidence angle (°)
C_{CPC}: Concentration ratio (-)
r_{out} : Outlet aperture radius (m)
r_{in} : Inlet aperture radius (m)
f: Focal distance (m)
L_{CPC}: 3D-CPC lenght (m)
$L_{CPC,T}$: 3D-CPC truncated length (m)
v_n : Normal vector (-)
ϕ_T : Truncated angle (°)

Abbreviations.

3D-CPC: Three-dimensional Compound Parabolic Concentrator
2D-CPC: Two-dimensional Compound Parabolic Concentrator
MCRT: Monte Carlo Ray Tracing
CSP: Concentrating Solar Power
STPP: Solar Tower Power Plant
DC: Dish Concentrator
SAM: System Advisor Model

Conflicts of Interest
The authors declare no conflict of interest.

Acknowledgements. We thank the academic authorities of the Alioune Diop University of Bambey and the Polytechnic School of Dakar for their support.

References

1. Kalogirou, S.A.: Solar thermal collectors and applications. Progr. Energy Combus. Sci. **30**, 231–295 (2004)
2. Huang, Y., Ma, X., Rao, C., Liu, X., He, R.: An annular compound parabolic concentrator used in tower solar thermal power generation system. Sol. Energy **188**, 1256–1263 (2019)

3. Shahabuddin, M., Alim, M.A., Alam, T., Mofijur, M., Ahmed, S.F., Perkins, G.: A critical review on the development and challenges of concentrated solar power technologies. Sustain. Energy Technol. Assess. **47**, 101434 (2021)
4. Malan, A., Kumar, K.R.: A comprehensive review on optical analysis of parabolic trough solar collector. Sustain. Energy Technol. Assess. **46**, 101305 (2021)
5. Tsegaye, S., Shewarega, F., Bekele, G.: A review on security constrained economic dispatch of integrated renewable energy systems. In: EAI Endorsed Transactions Conference 2020 on Energy Web, vol. 8, no. 32 (2021)
6. Xu, R., Ma, Y., Yan, M., Zhang, C., Xu, S., Wang, R.: Effects of deformation of cylindrical compound parabolic concentrator (CPC) on concentration characteristics. Sol. Energy **176**, 73–86 (2018)
7. Tian, M., Su, Y., Zheng, H., Pei, G., Li, G., Riffat, S.: A review on the recent research progress in the compound parabolic concentrator (CPC) for solar energy applications. Renew. Sustain. Energy Rev. **82**, 1272–1296 (2018)
8. Chandan, S.D., Kumar, P.S., Reddy, K.S., Pesala, B.: Optical and electrical performance investigation of truncated 3X nonimaging low concentrating photovoltaic-thermal systems. Energy Conv. Manag. **220**, 113056 (2020)
9. A. Ustaoglu, J. Okajima, X. Zhang and S. Maruyama.: Truncation effects in an evacuated compound parabolic and involute concentrator with experimental and analytical investigations, Applied Thermal Engineering, 17, 1359–4311 (2018)
10. Li, L., Wang, B., Pottas, J., Lipiński, W.: Design of a compound parabolic concentrator for a multi-source high-flux solar simulator. Sol. Energy **183**, 805–811 (2019)
11. Pozivil, P., Ettlin, N., Stucker, F., Steinfeld, A.: Design and experimental testing of a 50 kWth pressurized-air solar receiver for gas turbines. J. Solar Energy Eng. **137**, 0310021 (2015)
12. Jadhav, A.S., Gudekar, A.S., Patil, R.G., Kale, D.M., Panse, S.V., Joshi, J.B.: Performance analysis of a novel and cost effective CPC system. Energy Conv. Manag. **66**, 56–65 (2013)
13. Ustaoglu, A., Alptekin, M., Okajima, J., Maruyama, S.: Evaluation of uniformity of solar illumination on the receiver of compound parabolic concentrator (CPC). Sol. Energy **132**, 150–164 (2016)
14. Winston, R.: Principles of solar concentrators of a novel design. Sol. Energy **16**, 89–95 (1974)
15. Rabl, A.: Comparison of solar concentrators. Sol. Energy **18**, 93–111 (1976)
16. Dai, G., Xia, X., Sun, C., Zhang, H.: Numerical investigation of the solar concentrating characteristics of 3D CPC and CPC-DC. Sol. Energy **85**, 2833–2842 (2011)
17. Lipinski, W., Steinfeld, A.: Annular compound parabolic concentrator. J. Solar Energy Eng. **128**, 121–124 (2006)
18. Li, L., Wang, B., Pye, J., Lipinski, W.: Temperature-based optical design, optimization and economics of solar polar-field central receiver systems with an optional compound parabolic concentrator. Sol. Energy **206**, 1018–1032 (2020)
19. Wendelin, T.: SolTrace: a new optical modeling tool for concentrating solar optics. In: ASME 2003 Solar Energy Conference, Kohala Coast, HI (2003)
20. Winston, R., Miñano, J.C., Benítez, P.: Non-imaging Optics. Elsevier Academic Press, Cambridge (2005)
21. BarrónDíaz, J.E., et al.: FEM-CFD simulation and experimental study of compound parabolic concentrator (CPC) solar collectors with and without fins for residential applications. Appl. Sci. **11**, 3704 (2021)
22. Indira, S.S., Vaithilingam, C.A., Sivasubramanian, R., Chong, K., Saidur, R., Narasingamurthi, K.: Optical performance of a hybrid compound parabolic concentrator and parabolic trough concentrator system for dual concentration. Sustain. Energy Technol. Assess. **47**, 10538 (2021)

23. Slootweg, M., Craig, K.J., Meyer, J.P.: A computational approach to simulate the optical and thermal performance of a novel complex geometry solar tower molten salt cavity receiver. Sol. Energy **211**, 1137–1158 (2020)
24. Craig, K.J., Slootweg, M., Le Roux, W.G., Wolff, T.M., Meyer, J.P.: Using CFD and ray tracing to estimate the heat losses of a tubular cavity dish receiver for different inclination angles. Sol. Energy **211**, 1137–1158 (2020)
25. Wang, Y., et al.: Verification of optical modelling of sunshape and surface slope error for concentrating solar power systems. Sol. Energy **195**, 461–474 (2020)
26. Faye, K., Thiam, A., Faye, M.: Optimum height and tilt angle of the solar receiver for a 30 KWE solar tower power plant for the electricity production in the Sahelian Zone. Int. J. Photoenergy. 1961134 (2020)